Oscillations of photoconductivity and negative absolute conductivity in quantum wires

1993 J. Phys.: Condens. Matter 5 2233

(http://iopscience.iop.org/0953-8984/5/14/019)

J. Phys.: Condens. Matter 5 (1993) 2233–2254. Printed in the UK

Oscillations of photoconductivity and negative absolute conductivity in quantum wires

R Mickevičius†, V Mitin†, Michael A Stroscio‡ and M Dutta§

† Department of Electrical and Computer Engineering, Wayne State University, Detroit, MI 48202, USA

‡ US Army Research Office, PO Box 12211, Research Triangle Park, NC 27709, USA

§ US Army Electronics Technology and Devices Laboratory, SLCET-ED, Ft. Monmouth, NJ 07703-5601, USA

Received 15 September 1992, in final form 4 January 1993

Abstract. The phenomenon of oscillating photoconductivity as a function of photoinjection energy is studied by Monte Carlo simulation in quasi-one-dimensional quantum wire structures. It is demonstrated that the amplitude of the oscillations of photoconductivity may be so large that this leads to a negative absolute conductivity at injection energies that are multiples of the optical phonon energy. These oscillations are associated with inelastic optical phonon scattering, leading to an asymmetric electron distribution function established under conditions of intensive electron photoinjection to the subband bottom or close to energies that are multiples of the optical phonon energy. Simulation results suggest that quasi-one-dimensional quantum wires are ideal for the experimental observation of negative absolute conductivity at low lattice temperatures. To achieve negative conductivity at room temperature one needs extremely high recombination rates. The oscillations of photoconductivity can reveal the spectrum of optical phonons in quantum wires, which differs considerably from that in bulk materials.

1. Introduction

In addition to the now common phenomenon of negative differential conductivity in semiconductors there exists a rarer class of phenomena known as negative absolute conductivity. The first effect of negative absolute conductivity (NAC) due to a negative effective mass was predicted by Krömer [1]. Furthermore, the theory of this effect has been developed [2–4] and this effect has been observed experimentally [5,6]. Ultimately, NAC has yielded microwave generation due to a negative effective mass, as first observed by Andronov *et al* [7]—the goal that had been initially defined by Krömer [1].

Another mechanism of NAC has been predicted independently by Elesin and Manykin [8,9] and Stocker [10]. This effect is predicated on the existence of a considerably asymmetric electron distribution function under conditions of strong photoexcitation and recombination. If electrons are injected close to the optical phonon energy the electron distribution forms a spherical surface (shell) in k-space. An applied electric field will shift the electron distribution shell. Therefore, electrons with positive longitudinal components of wavevector k (against the electric field) will gain energy and enter (or stay in) the active region (here and later on the active and passive regions stand for the regions above optical phonon energy and below

0953-8984/93/142233+22$07.50

it, respectively). These electrons will be scattered down to the conduction band bottom by the emission of optical phonons. The electrons with negative longitudinal components of the k-vector will be shifted down to lower energies, will enter (or stay in) the passive region below optical phonon energy and cannot undergo optical phonon emission. As a result, electrons with negative velocity prevail over those with positive velocity and, accordingly, the drift velocity becomes negative, i.e. absolute negative conductivity is realized. Intensive recombination is required to eliminate electrons accumulated at the band bottom. However, it is almost impossible to realize this type of NAC in bulk materials, because of the rapid randomization of the three-dimensional electron momentum due to electron–electron, acoustic phonon and ionized impurity scattering, as well as electron penetration deep into the active region and heating of low-energy electrons. That is why NAC has never been observed experimentally although a lot of experimental efforts have been reported [11–16]. The only effect that has been observed is oscillating photoconductivity as a function of injection energy with period equal to optical phonon energy [11–16], but the minimum photoconductivity has never reached negative values.

A similar effect in crossed electric and quantizing magnetic fields has been predicted [17]. This case was realized experimentally by Aleksandrov *et al* [18]. The resonant nature of photocurrent dependence on photoexcitation energy was observed due to the above-mentioned effect, but NAC was not achieved [18]. The absence of NAC might be due to several reasons: (i) the presence of a hole current in interband photoexcitation [18], (ii) deep electron penetration into the active region, and (iii) the spread of the photoexcitation energy (and hence the electron energy). The difficulties of experimentally realizing NAC in bulk semiconductors are not easy to overcome and they may account for the fact that negative absolute photoconductivity has not gained wide recognition and has been disregarded for years. An exception was the paper by Reklaitis [19], where he proposed that in contrast to NAC at zero frequency, negative dynamic conductivity at high frequencies can be more easily realized. Due to inertia of the heating of low-energy electrons by high-frequency electric fields, these electrons do not contribute much to the conductivity. This fact removes the requirement of high recombination rates. But the severe restrictions on electron injection energy and lattice temperature make it extremely difficult to observe this effect experimentally. The situation has changed substantially with the revolutionary progress in modern semiconductor technology permitting the fabrication of the so-called quasi-one-dimensional (1D) quantum wire (QWI) structures.

In the present work, we demonstrate the possibility of realizing the effect of the NAC and the similar effect with photoexcitation to the bottom of the first subband in quasi-1D QWI. We demonstrate that QWIs are almost ideal structures for the observation of NAC. We have studied both transient and steady-state negative conductivity. Numerical results are obtained by the Monte Carlo technique for a rectangular GaAs QWI embedded in AlAs.

2. The origin of negative absolute conductivity

In this section we will consider a model of the NAC in QWI. In principle, the physical picture given below is true to some extent for bulk materials as well. QWIs present ideal, or at least very favourable, conditions for the effect of NAC for several reasons: (i) electrons in QWIs have no transverse components of velocity obstructing the

observation of these phenomena, and (ii) the longitudinal optical phonon emission rate is very high in the active region threshold [20,21] so that electrons are prevented from penetrating deeply into the active region. However, the key advantage of a QWI over a bulk material is the unique character of carrier scattering in 1D structures. As a result of the resonant behaviour of the density of states, the rates of electron scattering in the passive region (acoustic phonon and ionized impurity scattering as well as absorption of optical phonons) decrease dramatically as the electron kinetic energy increases. Electron–electron scattering in single-subband 1D structures involves merely an exchange of momenta between two indistinguishable electrons and obviously neither leads to the relaxation of electron momentum nor influences the electron transport at all [22]. Very recently there appeared a report by Fasol and Sakaki [23], where the authors predicted electron–electron scattering within the first subband if spin degeneracy of the GaAs conduction band was taken into account. This scattering can be suppressed by injecting only spin-up polarized electrons [23]. It is, however, too early to evaluate the effect of spin-related electron–electron scattering on electron transport characteristics. Hence, electron momentum randomization at the threshold of the active region is slow and does not prevent, accordingly, the realization of NAC. Furthermore, strong electron scattering by acoustic phonons close to the subband bottom may play a favourable role in the effect since it delays the heating electrons by an electric field.

Let us first consider the negative photoconductivity that occurs in the transient regime. We will consider two cases: (a) when electrons are injected to the first subband bottom at high lattice temperatures and (b) when electrons are injected with energy just below the optical phonon energy $\hbar\omega_0$ at low lattice temperatures. Case (a) has never been considered before, since it requires that the optical phonon absorption rate be sufficiently high, whereas all previous studies have been restricted to the case of low temperatures where optical phonon absorption is negligible. Due to rapid absorption of optical phonons, electrons enter the active region just above the optical phonon energy and form the same distribution as in the case of direct injection of electrons slightly above phonon energy. Therefore, the latter two cases (injection at zero energy and just above the optical phonon energy) are physically identical at high temperatures and we can consider them as variants of case (a).

Let the electric field be applied to an almost empty QWI (with negligible concentration of equilibrium carriers). Practically no current will flow through the wire. Suddenly electrons are injected into the first subband bottom (area 1, figure 1(a)) or just below the optical phonon energy (area 1, figure 1(b)). After injection to the subband bottom, electrons at high temperatures absorb optical phonons and enter the active region just above the optical phonon energy (area 2, figure 1(a)). The electric field drives electrons (deeper) into the active region on the positive side of the k-axis and out of (or away from) the active region on the negative side of the k-axis (area 3, figure 1). Due to fast optical phonon emission, electrons from the positive side of the k-axis almost instantaneously scatter down to the subband bottom. That is why the peak represented by area 3 in figure 1 represents only a brief transient electron distribution and it disappears during optical phonon emission time (10^{-14} s). The electrons in the negative part stay for a while, until being decelerated by an electric field or until their momentum is randomized by multiple scattering events. During this time, electrons with high negative velocity prevail over those with positive velocity. (The distribution function in both cases is qualitatively the same at this stage as shown by the dashed areas in figure 1(a) and

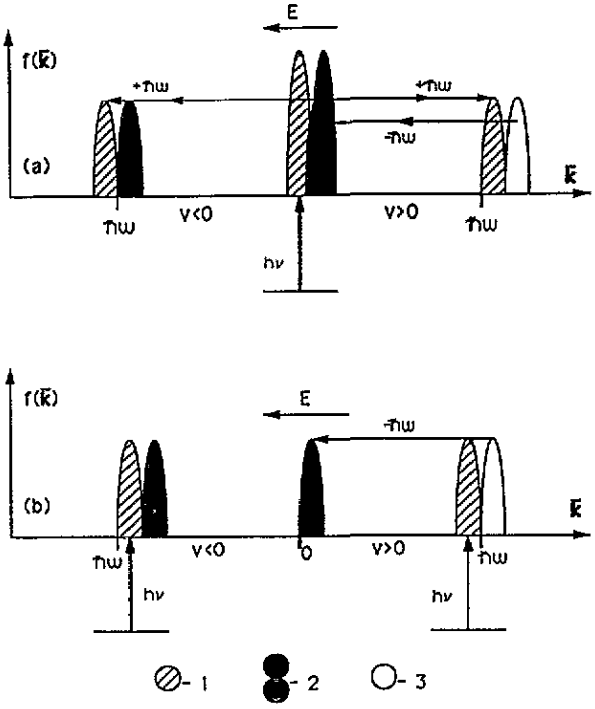

Figure 1. Schematic illustration of the formation of the electron distribution function responsible for the NAC. (*a*) High lattice temperatures and electron injection right to the first subband bottom. (*b*) Low temperatures and injection just below the optical phonon energy. Arrows show electron transfer channels due to absorption ($+\hbar\omega_o$) or emission ($-\hbar\omega_o$) of optical phonons. The electric field drags the electron system towards the positive side (right-hand side) of the k-axis (velocity axis). Area 1 is an initial electron distribution: (*a*) after electron injection and subsequent phonon absorption, (*b*) just after injection; area 2 is a final electron distribution after the shift by the electric field and emission of optical phonons; area 3 represents the virtual electron peak above the optical phonon energy (after the shift by the electric field but just before scattering down by emission of optical phonons).

(*b*)). As a result, the electron drift velocity is negative. The electric field has to be sufficient to extract electrons from the negative part of the active region before they emit optical phonons.

In order to get the effect of NAC in steady state we have to eliminate electrons from the low-energy region before they are heated (accelerated) by the electric field and can contribute to the positive part of the conductivity. The electrons that are eliminated must be replaced by injecting new electrons. The elimination mechanism we considered is linear recombination. (It might be electron extraction through contacts, as well, but we have not considered this case yet.) At a sufficiently high electron recombination rate, which will be defined in due course, the electron steady-state distribution function is similar to that shown in figure 1, i.e. it has three asymmetric peaks. (The low-energy peak can be only slightly pronounced when electrons are injected close to the phonon energy and the recombination rate is high. At high temperatures, there exist more peaks at energies that are multiples of the optical phonon energies and correspond to electron energies in different

subbands. They do not play the determinant role in conductivity formation.) For the realization of NAC at steady state, the recombination rate must be such that electrons recombine primarily during the regime of transient negative conductivity, i.e. the rate of recombination must be comparable with the rate of the dominant electron scattering mechanism or the electron heating rate by the electric field, whichever is higher. In that case, the electron distribution function is determined more by generation–recombination, together with electron scattering by optical phonons, than by scattering and heating by the electric field.

The effect of NAC may take place not only when electrons are injected close to the phonon energy (or zero, at high temperatures) but also if they are injected with energy close to an energy that is a multiple of the optical phonon energy. That is why we may observe oscillating photoconductivity as a function of injection energy with minima located at energies equal to optical phonon energies. This effect was widely studied experimentally in the 1960s [11–16]. In QWIs it is particularly interesting as a result of the presence of several optical phonon modes, namely confined longitudinal optical phonons and two surface, or interface, optical phonon modes all with different energies and couplings with electrons [20,21]. Therefore, it is possible to experimentally derive optical phonon energies and their coupling constants with electrons directly from the measurements of the photoconductivity–injection-energy dependence.

3. Model

We have examined a rectangular GaAs QWI embedded in AlAs. The model of the QWI includes multi-subband structure (up to 12 subbands) and 1D electron intrasubband and intersubband scattering by confined longitudinal-optical (LO) and localized surface-optical (SO) phonons [20,21]. Two SO phonon modes, GaAs-like and AlAs-like, are taken into consideration. The expressions for the scattering rates are given in appendix A. The dimensions of the QWI are chosen to be $150 \times 250\,\text{Å}^2$. The calculations have been performed by both the ensemble and single-particle Monte Carlo techniques. For the investigation of transient negative conductivity, electrons were 'injected by a short laser pulse' to the bottom of the first subband and the time evolution of the electron distribution was simulated by the ensemble Monte Carlo technique until the steady state was reached. The electron recombination was not included in these transient-regime simulations. When studying the steady-state regime by the single-particle Monte Carlo technique, the recombination of electrons was taken into account. An electron was injected into the subband bottom or close to the LO phonon energy and its motion was simulated until it recombined. After recombination the next electron was injected and the procedure repeated. Then the results were time averaged. To the best of our knowledge, there exist no data on hot electron recombination in QWIs. This is why we have used two simplified recombination models: one with an energy-independent (constant) recombination rate R_0 and another with a step-like energy dependence of recombination rate—equal to a constant value R_1 below some cutoff energy ϵ_1, and equal to zero above ϵ_1. The latter model is obviously more realistic since the probability of electron recombination decreases dramatically with increasing electron velocity (kinetic energy). Fortunately, this more realistic model enhances our effect. It is not desirable to eliminate electrons from the upper energies, which make the main contribution to the negative drift

velocity; it is necessary to exclude electrons with randomized momenta accumulated at lower energies and prevent their heating (acceleration) by an electric field and participation in the conduction. The cutoff energy ϵ_1 is chosen to be slightly above half of the LO phonon energy and is not a crucial parameter of the model. The recombination rate R_1 has been chosen in a wide range of 10^9–$10^{12}\,s^{-1}$, which practically covers experimental values in bulk materials. It seems to be desirable to have strong electron scattering at low energies (say, by acoustic phonons or by ionized impurities in the channel of the QWI or in the surrounding material) which can prevent electron heating in the passive region. We have included elastic scattering in our model with an average rate equal to the rate of electron scattering by acoustic phonons in bulk GaAs and decreasing as the inverse square root of electron kinetic energy. This scattering, however, does not play any role in the establishment of NAC, since it is weak at low temperatures (comparable with or lower than the recombination rate) and relatively weak at high temperatures (lower than the optical phonon absorption rate).

It must be mentioned here that real QWIs do not have perfect interfaces and constant thickness along a wire [21]. The effect of a variable cross section might have two consequences: additional elastic electron scattering by interface (surface) roughnesses [24] and disappearance of the coherent (resonant) nature of electron scattering by optical phonons [21]. The latter effect is analogous to the initial broadening of injected electron distribution and should not affect strongly NAC at low temperatures, where precision of injection is not so important. The electron scattering by interface roughnesses is important inasmuch as it is effective at higher electron energies (of the order of the optical phonon energy). The intensity of this scattering, however, strongly depends on technological processes used to fabricate a QWI, so that this scattering could be taken into consideration only for some particular QWI with known interface quality, but not in general.

4. Results and discussion

In this section we present results of the Monte Carlo simulation of NAC at two lattice temperatures: $T = 300\,K$ and $T = 10\,K$. These are the limiting cases of high and low temperatures, respectively. We have also performed simulations for $T = 77\,K$, which is the case of intermediate temperatures for NAC. The results obtained for $T = 77\,K$ are qualitatively the same as those for $T = 30\,K$, but at higher temperatures the range of electric fields where NAC appears is shifted up.

4.1. Results at $T = 300\,K$

First, we will consider the effect of the NAC in the transient regime. Figure 2 demonstrates that electrons injected in the bottom of the first subband exhibit negative drift velocities for the case of moderate electric fields at the very beginning of electron transient response. This transient process lasts about 1–3 ps in the field range 100–$500\,V\,cm^{-1}$ (see figure 2). This effect takes place only under certain conditions. One requirement is that electrons must be injected within a narrow energy range (close to the subband bottom or optical phonon energy) in order to be extracted from the negative active region (for case (a)) or driven into the positive active region (for case

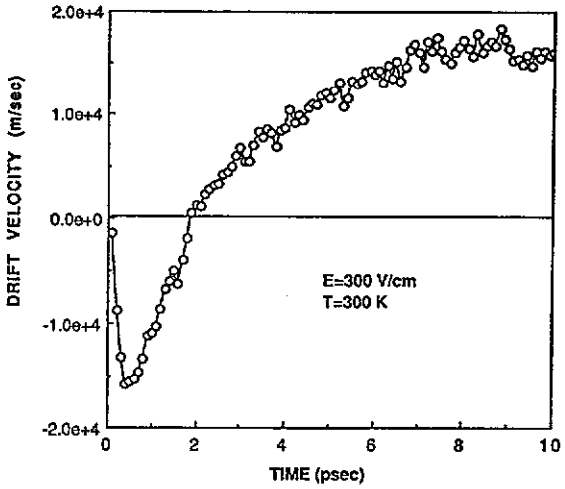

Figure 2. The transient response of the drift velocity following electron injection to the first subband bottom at $T = 300\,\mathrm{K}$, $E = 300\,\mathrm{V\,cm^{-1}}$. Recombination is not taken into account.

(b)) before they undergo scattering. This condition is given by

$$\Delta\epsilon < \frac{e^2E^2\tau^2}{m^*} \tag{1}$$

where τ stands for the average scattering time in the interval $\hbar\omega_o$–$2\hbar\omega_o$ (case (a)) or just below the optical phonon energy $\hbar\omega_o$(case (b)). It is obvious from (1) that the same requirement restricts the electric field E: it must be high enough to avoid severe restrictions on injected electron energies. However, in the case of injection just below the optical phonon energy, requirement (1) can be quite flexible inasmuch as the scattering time τ can be made long. Indeed, at low lattice temperatures the effective scattering time below the threshold of the active region in QWIs is several orders of magnitude larger than the effective time of optical phonon emission above $\hbar\omega_o$. Therefore, in case (b) the occurrence of the transient NAC does not crucially depend on injection energy.

On the other hand, the electric field must be low enough to prevent rapid heating of low-energy electrons and deep electron penetration into the active region. Otherwise negative transient conductivity can be on such a short timescale as to be unobservable. This requirement is given roughly by

$$E \ll \frac{\sqrt{2m^*\hbar\omega_o}}{e\tau}. \tag{2}$$

The fulfillment of both conditions (1) and (2) implies that $\Delta\epsilon/\hbar\omega_o \ll 1$.

We have already mentioned that the transient negative drift velocity lasts until low-energy electrons are heated sufficiently to make the dominant positive contribution to the conductivity or until the electron momentum is randomized by multiple scattering events. At room temperature the dominant scattering mechanism at low energies is longitudinal optical phonon absorption. Accordingly, the longitudinal optical phonon

absorption time defines the duration of the transient negative conductivity at 300 K and this transient regime should be short. It should be noted here that this effect is very inertialess at $T = 300$ K since it is defined by rather short scattering times. If we change the polarity of the electric field during transient negative conductivity the conductivity changes its sign within a time of the order of the time of optical phonon absorption ($< 10^{-12}$ s). (At low temperatures under injection of electrons just below the optical phonon energy, transient negative conductivity can last a long time depending upon the electric field. Its duration is defined by the electric field intensity, since it is responsible for heating of low-energy electrons which make a positive contribution to the total conduction. However, for small electric fields, the effect of NAC is less pronounced because the fields also determine the rate of electron transfer down to the subband bottom.)

At injection energies higher than defined by (1), the electron drift velocity does not reach negative values due to violation of the criterion (1), but double overshoot can be observed.

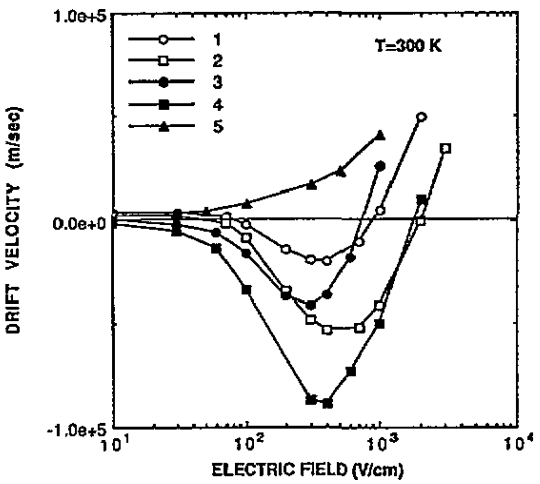

Figure 3. The steady-state electron drift velocity as a function of applied electric field at $T = 300$ K. Curve 1 is for a realistic QWI model with seven subbands and both LO and SO phonon modes and electron injection to the first subband bottom; curve 2 is for the same model but with electron injection at the LO phonon energy; curve 3 is for an ideal QWI with just a single subband and with only LO phonons taken into account, and electron injection to the subband bottom; curve 4 is for the same ideal QWI but with electron injection right at the LO phonon energy; and curve 5 is the dark electron (background) velocity. Curves 1–4 are obtained for the step-like recombination rate $R_1 = 2 \times 10^{12}\,s^{-1}$ below a cutoff energy $\epsilon_1 = 0.022$ eV.

For the investigation of steady-state negative conductivity we have employed a single-particle Monte Carlo simulation with electron recombination taken into account. Figure 3 illustrates the steady-state velocity–field dependences of injected electrons under intensive recombination. The recombination rate is assumed to be a step-like function of electron energy with a cutoff energy $\epsilon_1 = 0.022$ eV for the results presented in figure 3. The steady-state characteristics without recombination are plotted for comparison. NAC appears in a certain range of electric fields and at high

recombination rates. However, even when the velocity does not reach the negative values, it decreases with increasing electric field, i.e. in a certain range of electric fields the negative differential conductivity is realized. The range of fields where NAC appears at high recombination rates can be roughly estimated from inequalities (1) and (2). The existence of lower threshold fields for the occurrence of NAC is caused by the fact that we inject electrons not *exactly* to the subband bottom but 0.2 meV above it. As a result the field must be large enough to extract electrons from the negative part of the active region before they emit optical phonons. It is seen from figure 3 that the effect of NAC is more pronounced for electron injection close to the optical phonon energy than for injection to the subband bottom. The effect is also stronger when only one subband and only LO phonons are taken into account. The electric field range where NAC occurs for the latter idealized case is shifted down slightly.

The simulation results show that NAC occurs only if the recombination rate is sufficiently high, as has been discussed in section 2. The question is: how critical is the existence of NAC on the rate of recombination and on the model of recombination used? Figure 4 shows the drift velocity as a function of the recombination rate for real and idealized models of the QWI and for two electron injection energies. Most of the results are obtained within the step-like recombination model. The results of the calculation for constant recombination rate are presented as well. It is seen from figure 4 that the step-like recombination model yields a far stronger NAC effect, especially at higher recombination rates. The reason for this is that step-like recombination does not affect the electron distribution at higher energies, i.e. those electrons that are responsible for the existence of NAC. As a result, unlike within the constant recombination model, within the step-like model there exist no higher critical rates of recombination that could cause the disappearance of NAC. However, the recombination required to observe NAC at room temperature is extremely high, if not to say unphysically high (over $2 \times 10^{11}\,s^{-1}$). Even though the strong interface recombination in QWIS may be expected, the overall conclusion is that high temperatures are not favourable for observing NAC. (In the following subsection we will see that the conditions for observing NAC change completely at low temperatures.) Additional model simulations (not presented) have shown that when electron scattering in the passive region is stronger the effect of NAC is better pronounced, particularly at lower recombination rates.

The physical nature of NAC is seen clearly from figure 5, which shows an electron velocity distribution function under intensive injection to the subband bottom and step-like recombination. We see several peaks for both positive and negative velocities. They are related to LO and SO phonons (which have different energies) and electrons in the second subband. These additional peaks disappear when only one subband and only LO phonons are considered (compare figures 5 and 6). The electron population at the negative part of the velocity axis is larger than at the positive part, resulting in the appearance of NAC.

The existence of an unusual electron distribution in momentum space under intensive generation and recombination is also well pronounced in the energy distribution of electrons. Figure 7 depicts the energy distribution of electrons in a multi-subband QWI. One can see the pronounced peaks at energies that are multiples of the LO phonon energy. (The influence of SO phonons is not noticeable against the background of strong LO phonon effects, since the rate of electron scattering by LO phonons in a QWI of this size is more than an order of magnitude higher [21].)

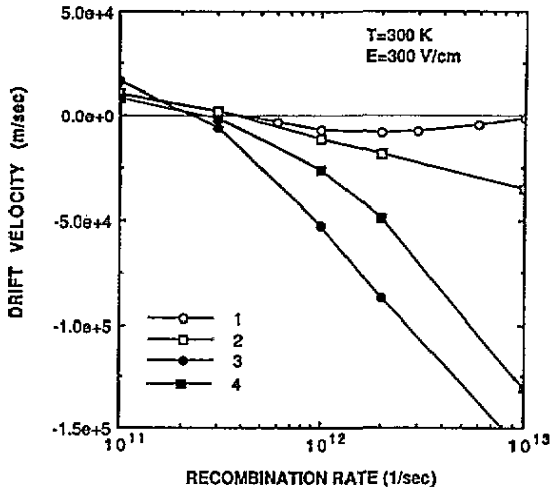

Figure 4. The steady-state electron drift velocity as a function of recombination rate. Curve 1 is for a realistic QWI model with seven subbands and account taken of both LO and SO phonons, but with a constant recombination rate R_0 independent of electron energy and electron injection to the first subband bottom; curve 2 is for the same QWI and injection model but with the step-like recombination rate R_1 with cutoff energy of 0.022 eV; curve 3 is for the same model as curve 2 except that injection is at the LO phonon energy; curve 4 represents a simplified single-subband model of a QWI when only LO phonons are taken into account, with electron injection at the LO phonon energy and step-like recombination.

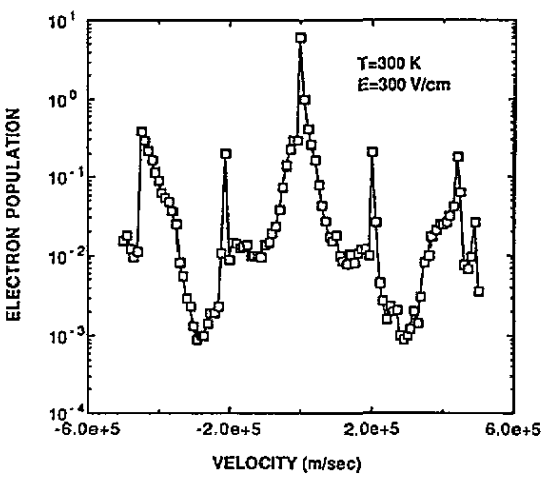

Figure 5. Electron steady-state velocity distribution for a realistic QWI model with seven subbands and both LO and SO phonons and a step-like recombination rate $R_1 = 10^{13}\,s^{-1}$. The injection energy is equal to zero.

The regions with a negative derivative of the distribution function with respect to electron energy present evidence of the existence of negative conductivity. In the case when recombination and permanent injection are not included the distribution

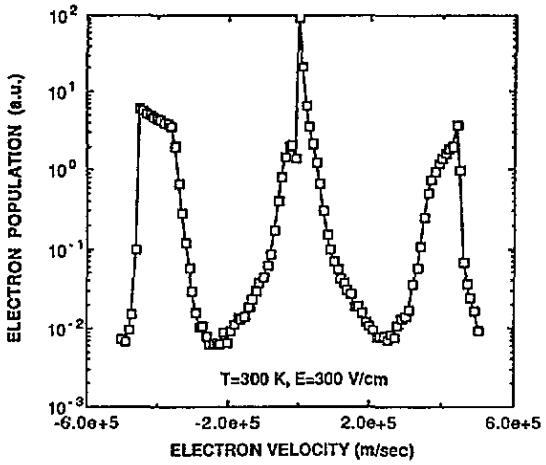

Figure 6. Electron steady-state velocity distribution for a simplified single-subband QWI model with account taken of only LO phonons and the same recombination rate and injection energy as in figure 5.

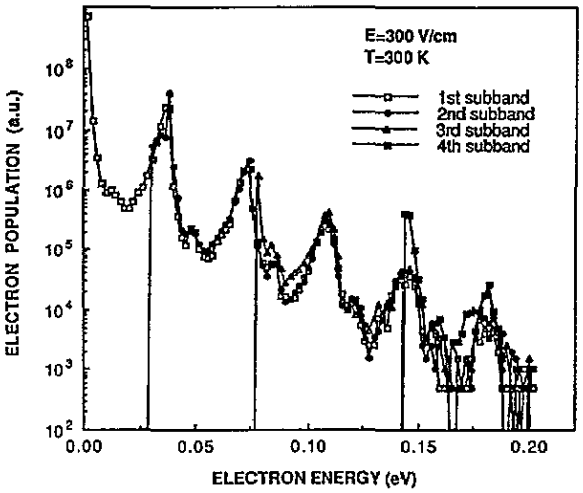

Figure 7. Electron steady-state energy distribution for a multi-subband QWI. The recombination rate here is assumed to be energy independent and equal to $2 \times 10^{12}\,s^{-1}$. The electron injection energy is equal to zero.

function decreases monotonically as the electron energy increases.

It is important to mention here the oscillatory dependence of the conductivity on injection energy—an effect that has been observed experimentally many times. We have calculated this dependence for $T = 300\,K$ within the realistic seven-subband model of the QWI with both LO and SO phonons included. This dependence and the mean electron energy as a function of injection energy are presented in figure 8. The amplitudes of the oscillations of the electron velocity for this large recombination rate are large enough to get well pronounced regions with NAC. The lowest minimum on

the dependence is seen at the single energy of the LO phonon; this is in accordance with the most favourable condition for the occurrence of NAC. The shapes of the minima are asymmetric, with a steeper increase in conductivity above the (multiple) phonon energy. It is seen from figure 8(*b*) that the mean electron energy is also an oscillatory function of injection energy, i.e. relative cooling of the electron system is realized.

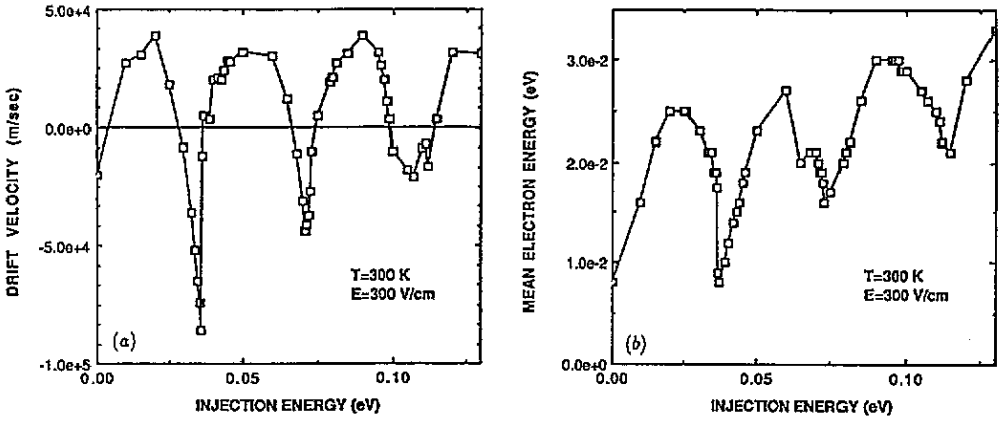

Figure 8. Electron drift velocity (*a*) and mean electron energy (*b*) as a function of injection energy for a multi-subband QWI with both SO and LO phonons taken into consideration. The recombination rate is step-like with a cutoff energy of 0.022 eV and a low-energy value $R_1 = 2 \times 10^{12}\,s^{-1}$.

4.2. Results at T = 10K

Low temperatures considerably modify the physical picture for the occurrence of NAC. At low temperatures, electrons can reach the active region only by means of heating by electric fields, or they must be injected directly above the optical phonon emission threshold. Moreover, scattering in the passive region is weak so that only heating of low-energy electrons affects the existence of NAC. Consequently, the role of the electric field increases significantly at low temperatures. The criterion for the observation of NAC at steady state follows straightforwardly from the requirement that the negative part of the electric current due to electrons injected with negative momenta is larger than the positive one defined by the heating of low-energy electrons and by the electrons with positive injected momenta. At very low temperatures when acoustic phonon scattering is weak and at low electric fields ($eE \ll Rp_i$) when electrons are injected below the optical phonon energy this criterion can be easily derived from the electron balance equations; the condition may be written as follows:

$$p_o e^{-R(p_o-p_i)/eE} + \frac{eE}{R} e^{-Rp_i/eE} > \frac{2eE}{R} \tag{3}$$

where p_i and p_o are magnitudes of the momenta corresponding to the electron injection energy and the optical phonon energy, respectively, and R is the recombination rate. The inequality (3) implies the need for a high ratio for R/E,

together with the minimum possible difference $(p_o - p_i)$. It the latter case, electrons in the low-energy region rather recombine than are heated (accelerated) by an electric field and electrons near injection energy form a narrow peak of the order of $(p_o - p_i)$ at positive velocities and a wide peak of the order of p_i at negative velocities.

The steady-state velocity–field dependence for $T = 10\,\mathrm{K}$ is presented in figure 9. All the simulations for $T = 10\,\mathrm{K}$ have been performed within the step-like recombination model with a cutoff energy of 0.022 eV above which the recombination rate is equal to zero. It is obvious from figure 9 that the effect is far stronger at high recombination rates. However, even in the case of a recombination rate as low as $2 \times 10^9\,\mathrm{s}^{-1}$, a region of NAC exists although the magnitude of the velocity is rather small. (At $T = 300\,\mathrm{K}$ and the same recombination rate, the electron velocity is positive in the entire region of the electric field). Curves 3 and 4 represent two different electron injection energies, just below the lower SO phonon energy and just below the LO phonon energy, respectively. It is seen from these curves that injection just below the SO phonon energy is better for the observation of NAC, since the electron scattering rate in that (passive) region is much lower than the scattering rate just below the LO phonon energy. It is seen from figure 9 that there exists no lower limit of electric field below which NAC disappears. This is due to the fact that electrons are injected right at the optical (LO or SO) phonon energy, so that even the weakest electric field is able to instantly extract electrons from the negative part of the active region. Certainly, in real conditions where the electron injection energy is spread over some finite interval, there exists the lower limit of electric fields.

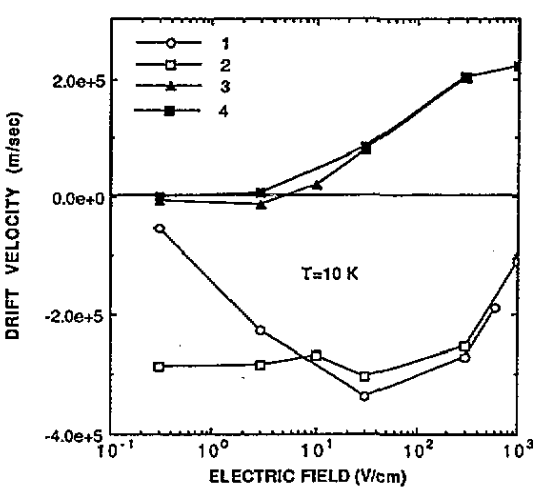

Figure 9. The steady-state electron drift velocity as a function of applied electric field at $T = 10\,\mathrm{K}$. Curve 1 is for the ideal QWI with just a single subband and with only LO phonons taken into account and electron injection at the LO phonon energy, $R_1 = 2 \times 10^{12}\,\mathrm{s}^{-1}$; curve 2 is for a realistic QWI model with seven subbands and both LO and SO phonon modes and electron injection at the LO phonon energy, $R_1 = 2 \times 10^{12}\,\mathrm{s}^{-1}$; curve 3 is for the same realistic model but with electron injection at the SO phonon energy and $R_1 = 2 \times 10^9\,\mathrm{s}^{-1}$; curve 4 is for the same model as curve 3 but with electron injection at the LO phonon energy.

To get NAC at $T = 300\,\mathrm{K}$ it was necessary to have a very large recombination rate. At $T = 10\,\mathrm{K}$ this requirement is dramatically relaxed. One can see from figure 9

that NAC at 10K occurs at recombination rates *three orders of magnitude lower* than at $T = 300$K. The point is that electron scattering in the passive region is so weak that it does not lead to momentum randomization of electrons contributing to conductivity. The only obstacle now is electron heating by an electric field in the passive region (as has been discussed above). Roughly speaking, the heating rate must be lower than the recombination rate in order to observe NAC. Consequently, the intensity of the electric field in this case defines the critical recombination rate required to get NAC.

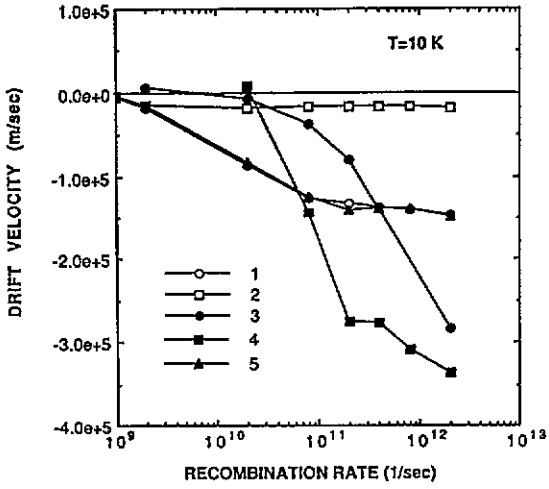

Figure 10. The steady-state electron drift velocity as a function of recombination rate. Curve 1 represents a simplified single-subband model of a QWI when only LO phonons are taken into account, with electron injection at the LO phonon energy, $E = 3\,\mathrm{V\,cm^{-1}}$; curves 2 and 4 are for the same simplified model but for $E = 0.3\,\mathrm{V\,cm^{-1}}$ and $E = 30\,\mathrm{V\,cm^{-1}}$, respectively; curve 3 is for the realistic QWI model with seven subbands and account taken for both LO and SO phonons and electron injection at the LO phonon energy, $E = 3\,\mathrm{V\,cm^{-1}}$; curve 5 is for the same realistic QWI model except that injection is at the SO phonon energy, $E = 3\,\mathrm{V\,cm^{-1}}$. The recombination rate for all curves is taken to be step-like and energy dependent with a cutoff energy of 0.022eV.

Figure 10 shows the dependence of the drift velocity on the recombination rate at $T = 10$K. Indeed, unlike in the case of high temperatures, negative conductivity occurs even at low recombination rates. It is evident from figure 10 that the lower the electric field, the lower the recombination rate required to observe negative conductivity—a result that has been expected from simple considerations (more strictly the lower limit of recombination rate is defined by (3), where the recombination rate and electric field always appear only as a ratio R/E). At higher electric fields, however, the magnitude of the negative conductivity is larger. One can see from figure 10 that velocity–recombination-rate dependences virtually coincide for the two different cases represented by curves 1 and 5. In fact, electron penetration into the active region above the optical phonon energy (LO or SO) is negligible *at that low electric field* and so is their transfer to the upper subbands. Therefore, electron injection just below the SO phonon energy (curve 5) or just below the LO phonon energy *in the absence of SO phonons* (curve 1) lead to the same consequences regardless of the upper subbands.

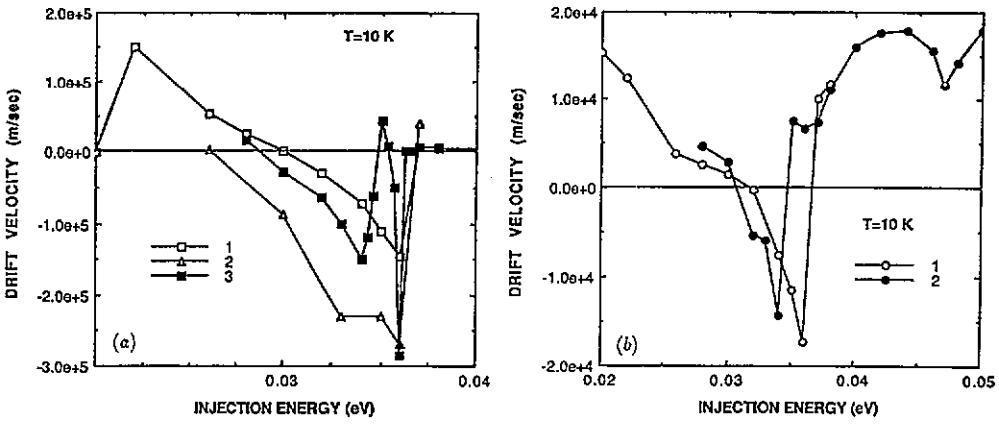

Figure 11. Electron drift velocity as a function of injection energy at $T = 10\,\mathrm{K}$. (*a*) Curves 1 and 2 are for the simplified single-subband QWI model with account taken of only LO phonons and with a step-like recombination rate $R_1 = 2 \times 10^{12}\,\mathrm{s}^{-1}$ and $E = 3\,\mathrm{V\,cm}^{-1}$ or $E = 300\,\mathrm{V\,cm}^{-1}$, respectively; curve 3 is for the realistic seven-subband model with both SO and LO phonons taken into account, $R_1 = 2 \times 10^{12}\,\mathrm{s}^{-1}$, $E = 3\,\mathrm{V\,cm}^{-1}$. (*b*) Curve 1 is for a single-subband model with account taken for only LO phonons, and curve 2 is for a multi-subband model with both SO and LO phonons included; for both curves $R_1 = 2 \times 10^{9}\,\mathrm{s}^{-1}$, $E = 3\,\mathrm{V\,cm}^{-1}$. The recombination rate for all curves is taken to be step-like and energy dependent with a cutoff energy of 0.022 eV.

Of particular importance is the oscillatory dependence of the photoconductivity as a function of injection energy since it reflects all possible phonon modes in QWIs. For $T = 10\,\mathrm{K}$ we have calculated this dependence for a realistic multi-subband QWI with all phonon modes taken into account. For comparison we also calculated these dependences for a simplified model of the QWI. Figure 11 demonstrates the drift velocity as a function of injection energy for different electric fields and QWI models. It is seen from this figure that there exists just one minimum in the case of an ideal QWI model corresponding to the energy of the LO phonon. In the case of a real QWI, two or even three (see curve 2 in figure 11(*b*)) minima appear on the dependence reflecting different phonon modes: SO modes at 0.034 eV and 0.044 eV as well as an LO mode at 0.036 eV. The different depths of the minima reflect the different electron scattering rates by various phonon modes as well as the different scattering times in the regions below corresponding phonon energies. The local minimum on that dependence related to LO phonon energy is strongly pronounced at high recombination rates (figure 11(*a*), curve 3) and only slightly pronounced at low recombination rates (figure 11(*b*), curve 2). In fact, electrons are already in the active region (above the SO phonon energy) when they are just below the LO phonon energy. Therefore, a fraction of these electrons is scattered down by emission of SO phonons. However, if the recombination rate is comparable or higher than the SO phonon emission rate, electrons that are scattered down rapidly recombine and do not accumulate in the low-energy region. This is why at sufficiently high recombination rates the electron distribution virtually does not sense the scattering down by SO phonons. The minima with NAC at $T = 30\,\mathrm{K}$ are rather wide so that there are no severe restrictions on injection energy. A thorough analysis of the experimentally obtained dependences could reveal the actual picture of electron scattering by confined and localized phonons in QWIs. Had the experimental data been

available, we could have performed a more detailed analysis of these dependences.

We have already mentioned that the electric field plays a decisive part (together with the recombination rate) in the formation of the distribution function at low temperatures. In order to demonstrate clearly that role we have performed several simulations with different R/E ratios at the same injection energy. For the sake of refinement of pure electric-field effects we have used the simple single-subband model of the QWI with only LO phonons considered. Figure 12 depicts the electron velocity distribution for two applied electric fields and for a step-like recombination rate $R_1 = 2 \times 10^{12}\,\mathrm{s}^{-1}$. At high electric fields (figure 12(a)) electron transfer down to the subband bottom is sufficiently high and results in the appearance of the peak at $v = 0$ (electrons do not manage to recombine that fast). The peak at the positive injection velocity, however, almost completely disappears. In the case of low electric fields (figure 12(b)) the situation is the opposite: all slow electrons that are being transferred down to the subband bottom, recombine there. Therefore, the peak at $v = 0$ is not noticeable but the peak at positive velocity is strongly pronounced, reflecting the bottleneck of the electron transfer down.

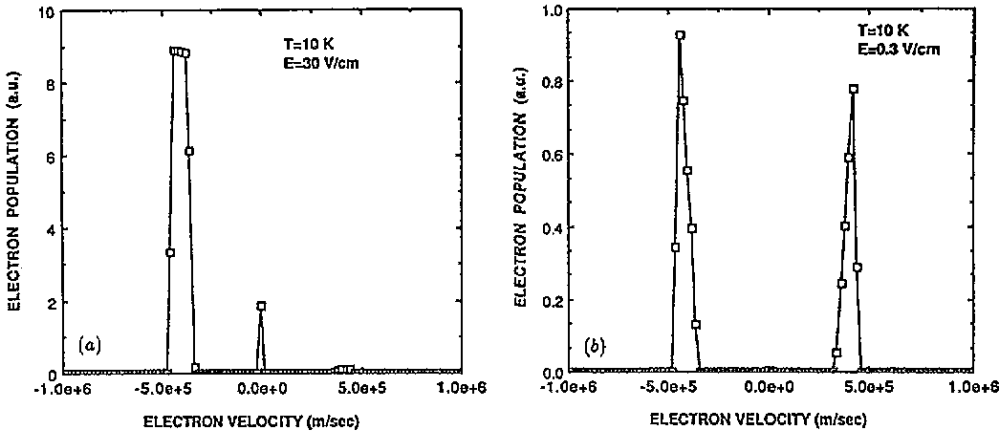

Figure 12. Electron steady-state velocity distribution for a simplified single-subband QWI model with account taken of only LO phonons at (a) $E = 30\,\mathrm{V\,cm}^{-1}$ and (b) $E = 0.3\,\mathrm{V\,cm}^{-1}$. The recombination rate is step-like and energy dependent: $R_1 = 2 \times 10^{12}\,\mathrm{s}^{-1}$ with a cutoff energy $\epsilon_1 = 0.022\,\mathrm{eV}$.

5. Summary and conclusions

We have demonstrated that the electron photoconductivity oscillations in QWIs as a function of injection energy may lead to NAC in the vicinity of the optical phonon energy and at energies that are multiples of the LO phonon energy. At high lattice temperatures, NAC may also appear at zero injection energy as a result of rapid absorption of optical phonons and their subsequent re-emission. We have demonstrated that QWIs have scattering processes that are well suited for the occurrence of NAC, especially at low temperatures. On the other hand, the oscillatory dependence of photoconductivity on the injection energy contains all the information

on electron scattering by confined and localized phonons in QWIs. Consequently, this information can be revealed from an analysis of experimental dependences. This may be an indirect experimental technique for studying peculiarities of the optical phonon spectrum in low-dimensional structures.

We have used a somewhat simplified model and have not specified where electrons are injected from and what is the recombination mechanism. If we deal with interband photoexcitation, holes should be included in the model. However, due to low hole mobility in GaAs, their contribution to the total current would be negligible. Moreover, electrons can be photoexcited from impurity levels. In this case electron ionized impurity scattering should be considered. But we already know from model simulations that this low-energy scattering may only improve the effect. Electrons with zero energy cannot be injected from the surrounding material but they can, in principle, be injected with the optical phonon energy under certain conditions, so that we can consider electron injection from the surrounding material as a possible way to generate electrons in our system. Required recombination rates are very high at high temperatures. It seems that it is possible to achieve high recombination rates in QWIs due to the strong influence of interface traps. There might also be other mechanisms excluding passive electrons (say, extraction through the contacts). However, the necessity of strong recombination along with requirement of precise control over exiting photon energy makes room temperature less favourable for observing NAC than low temperatures. At $T = 10\,\mathrm{K}$ NAC occurs at recombination rates as low as $2 \times 10^9\,\mathrm{s}^{-1}$, i.e. by three orders of magnitude less than at room temperature.

If the recombination rate is not sufficient to reach negative drift velocities at room temperature, negative differential conductivity can be realized. It has been shown by Reklaitis [19] that negative conductivity can occur at high frequency even if it is not achievable at zero frequency in bulk materials. (This is true for QWIs as well.) This is due to the fact that, if the electric field frequency is sufficiently high, electrons in the passive region do not undergo scattering during the half-period of the electric field and they follow the field inertialessly. Therefore, there is no net heating of electrons in the passive region during the field period. However, the frequency of the electric field must be low enough to ensure electron scattering in the active region during a half-period. Hence, the negative dynamic conductivity can occur in the frequency range given by

$$\tau_p^{-1} < \frac{\omega}{2\pi} < \tau_e^{-1} \tag{4}$$

where τ_p is the effective scattering time in the passive region below the optical phonon energy and τ_e is the optical phonon emission time. The main obstacle to observing negative dynamic conductivity in bulk materials is the severe restriction of electron injection energy because of the requirement that electrons be injected slightly above the optical phonon energy where the derivative of phonon emission rate with respect to energy is very high [19]. However, in QWIs this obstacle can be obviated by electron injection below the optical phonon energy. Indeed, the electron scattering rate in the passive region just below optical phonon energy is much lower in a QWI in comparison with a bulk material at the same temperature. At low temperatures NAC occurs even at electron injection significantly below the optical phonon energy (see the wide minima with NAC in figure 11) as a result of slow randomization of electron momentum below the optical phonon energy. This is why the precision of electron injection is not of crucial importance in QWIs at low temperatures, and it makes low temperatures even more attractive.

Acknowledgment

The work of R Mickevičius and V Mitin was supported by ARO under grant no DAAL03-92-G-0044.

Appendix. Electron–phonon scattering rates

We assume a rectangular quantum wire with an infinitely deep quantum well. Let the direction x be along the quantum wire. In this case the one-dimensional electron wavefunction is of the well known form

$$|\, q_x, j, l\rangle = \frac{1}{\sqrt{L_x}} \exp(ik_x x)\sqrt{\frac{2}{L_y}} \sin\left(\frac{j\pi y}{L_y}\right) \sqrt{\frac{2}{L_z}} \sin\left(\frac{j\pi z}{L_z}\right) \qquad j = 1,2,\ldots \quad l = 1,2,\ldots \tag{A1}$$

and the corresponding energy is

$$E(k_x, j, l) = E_x(k_x) + E_{jl} \tag{A2}$$

where

$$E_x(k_x) = \frac{\hbar^2 {k_x}^2}{2m^*} \tag{A3}$$

is the electron kinetic energy, k_x is the free x-component of the electron wavevector, and

$$E_{jl} = \frac{\hbar^2}{2m^*}\left[\left(\frac{j\pi}{L_y}\right)^2 + \left(\frac{l\pi}{L_z}\right)^2\right] \tag{A4}$$

is the subband j, l energy with respect to the bulk ground level.

The transition probability from an initial electron state $|k_x, j, l\rangle$ to a final state $|k'_x, j', l'\rangle$ according to the Fermi golden rule is as follows:

$$W^{e/a}(k_x, j, l; k'_x, j', l') = \frac{2\pi}{\hbar}\, |M^{e/a}|^2\, \delta[E(k'_x, j', l') - E(k_x, j, l) \pm \hbar\omega] \tag{A5}$$

where the superscripts 'e' and 'a' indicate emission and absorption, respectively, and $M^{e/a}$ is the matrix element for the electron–phonon interaction:

$$M^{e/a} = \left\langle k'_x, j', l'; N + \tfrac{1}{2} \pm \tfrac{1}{2} | H^{1D} | q_x, j, l; N + \tfrac{1}{2} \mp \tfrac{1}{2} \right\rangle \tag{A6}$$

where H^{1D} is the Fröhlich Hamiltonian of 1D confined longitudinal optical (LO) or localized surface optical (SO) phonons. The expression for this Hamiltonian, derived within the dielectric continuum model, is given in [20]. Recent lattice dynamics calculations of phonon wavefunctions [25] give close agreement with sine

wavefunctions assumed within the dielectric continuum model. The total electron scattering rate from the state $|k_x, j, l\rangle$ to elsewhere can be expressed as

$$\lambda^{e/a}(k_x, j, l) = \sum_{j',l'} \lambda^{e/a}(k_x, j, l; j', l') \tag{A7}$$

where the rate of a particular intrasubband or intersubband $j, l \to j', l'$ transition is given by

$$\lambda^{e/a}(k_x, j, l; j', l') = \frac{e^2}{8\pi^2\epsilon_o} \int dq_x \; \omega(N + \tfrac{1}{2} \pm \tfrac{1}{2}) \; I(q_x, L_y, L_z) \times \delta[E(k_x', j', l') - E(k_x, j, l) \pm \hbar\omega_{LO}]\delta_{k_x', k_x \pm q_x} \tag{A8}$$

where I is the electron–phonon coupling factor. For LO phonons we have [20]

$$I_{LO}(q_x, L_y, L_z) = \left(\frac{1}{\kappa_\infty} - \frac{1}{\kappa_0}\right)\frac{2\pi^2}{L_y L_z} \times \sum_{m=1,2,3,\ldots} \sum_{n=1,2,3,\ldots} \left(\frac{4P_{mn}}{[q_x^2 + (m\pi/L_y)^2 + (n\pi/L_z)^2]^{1/2}}\right)^2 \tag{A9}$$

with the overlap integral between electron and phonon wavefunctions, P_{mn}, given by

$$P_{mn} = \frac{1}{4\pi^2}\left(\frac{(-1)^{l+l'+n} - 1}{l + l' + n} - \frac{(-1)^{l+l'-n} - 1}{l + l' - n} - \frac{(-1)^{l-l'+n} - 1}{l - l' + n} + \frac{(-1)^{l-l'-n} - 1}{l - l' - n}\right) \times \left(\frac{(-1)^{j+j'+m} - 1}{j + j' + m} - \frac{(-1)^{j+j'-m} - 1}{j + j' - m} - \frac{(-1)^{j-j'+m} - 1}{j - j' + m} + \frac{(-1)^{j-j'-m} - 1}{j - j' - m}\right). \tag{A10}$$

In (A9) we sum only over such phonon modes m and n that correspond to a non-zero denominator in (A10).

For SO phonons we have [20]

$$I_{SO}(q_x, L_y, L_z) = \left(\frac{2\pi C' P_{SO}}{\omega_{SO}}\right)^2.$$

The overlap integral P_{SO} for symmetric modes is given by

$$P_{SO}^s = \frac{jj' \sinh(\alpha L_y/2)[(-1)^{j+j'} + 1]}{\alpha L_y \cosh(\frac{1}{2}\alpha L_y)\{\frac{1}{2}(j^2 + j'^2) + (\alpha L_y/2\pi)^2 + (2\pi/\alpha L_y)^2[\frac{1}{4}(j^2 - j'^2)]^2\}} \times \frac{ll' \sinh(\beta L_z/2)[(-1)^{l+l'} + 1]}{\beta L_z \cosh(\frac{1}{2}\beta L_z)\{\frac{1}{2}(l^2 + l'^2) + (\beta L_z/2\pi)^2 + (2\pi/\beta L_z)^2[\frac{1}{4}(l^2 - l'^2)]^2\}} \tag{A11}$$

and for antisymmetric modes

$$P^{a}_{SO} = \frac{jj'\cosh(\alpha L_y/2)[(-1)^{j+j'}+1]}{\alpha L_y \sinh(\frac{1}{2}\alpha L_y)\{\frac{1}{2}(j^2+j'^2)+(\alpha L_y/2\pi)^2+(2\pi/\alpha L_y)^2[\frac{1}{4}(j^2-j'^2)]^2\}}$$
$$\times \frac{ll'\cosh(\beta L_z/2)[(-1)^{l+l'}+1]}{\beta L_z \sinh(\frac{1}{2}\beta L_z)\{\frac{1}{2}(l^2+l'^2)+(\beta L_z/2\pi)^2+(2\pi/\beta L_z)^2[\frac{1}{4}(l^2-l'^2)]^2\}}. \tag{A12}$$

The normalization constant C' for symmetric modes is given by

$$\begin{aligned} C'^{-2} = {} & \epsilon_1(\infty)\frac{(\omega_{l1}^2-\omega_{t1}^2)}{(\omega^2-\omega_{t1}^2)^2}[\cosh(\alpha L_y/2)\cosh(\beta L_z/2)]^{-2} \\ & \times\left[\frac{\alpha^2}{2}\left(\frac{L_z}{\alpha}\sinh(\alpha L_y)+\frac{\sinh(\alpha L_y)\sinh(\beta L_z)}{\alpha\beta}\right)\right. \\ & \left.+\frac{\beta^2}{2}\left(\frac{L_y}{\beta}\sinh(\beta L_z)+\frac{\sinh(\alpha L_y)\sinh(\beta L_z)}{\alpha\beta}\right)\right] \\ & +\epsilon_2(\infty)\frac{(\omega_{l2}^2-\omega_{t2}^2)}{(\omega^2-\omega_{t2}^2)^2}[\cosh(\alpha L_y/2)]^{-2} \\ & \times\left[\alpha^2\left(\frac{\sinh(\alpha L_y)}{\alpha\beta}\right)+\beta^2\left(\frac{\sinh(\alpha L_y)}{\alpha\beta}+\frac{L_y}{\beta}\right)\right] \\ & +\epsilon_2(\infty)\frac{(\omega_{l2}^2-\omega_{t2}^2)}{(\omega^2-\omega_{t2}^2)^2}[\cosh(\beta L_z/2)]^{-2} \\ & \times\left[\alpha^2\left(\frac{\sinh(\beta L_z)}{\alpha\beta}+\frac{L_z}{\alpha}\right)+\beta^2\left(\frac{\sinh(\beta L_z)}{\alpha\beta}\right)\right] \\ & +\epsilon_2(\infty)\frac{(\omega_{l2}^2-\omega_{t2}^2)}{(\omega^2-\omega_{t2}^2)^2}\left(\frac{2(\alpha^2+\beta^2)}{\alpha\beta}\right) \end{aligned} \tag{A13}$$

and for antisymmetric modes C' is given by

$$\begin{aligned} C'^{-2} = {} & \epsilon_1(\infty)\frac{(\omega_{l1}^2-\omega_{t1}^2)}{(\omega^2-\omega_{t1}^2)^2}[\sinh(\alpha L_y/2)\sinh(\beta L_z/2)]^{-2} \\ & \times\left[\frac{\alpha^2}{2}\left(\frac{L_z}{\alpha}\sinh(\alpha L_y)+\frac{\sinh(\alpha L_y)\sinh(\beta L_z)}{\alpha\beta}\right)\right. \\ & \left.+\frac{\beta^2}{2}\left(\frac{L_y}{\beta}\sinh(\beta L_z)+\frac{\sinh(\alpha L_y)\sinh(\beta L_z)}{\alpha\beta}\right)\right] \\ & +\epsilon_2(\infty)\frac{(\omega_{l2}^2-\omega_{t2}^2)}{(\omega^2-\omega_{t2}^2)^2}[\sinh(\alpha L_y/2)]^{-2} \\ & \times\left[\alpha^2\left(\frac{\sinh(\alpha L_y)}{\alpha\beta}\right)+\beta^2\left(\frac{\sinh(\alpha L_y)}{\alpha\beta}+\frac{L_y}{\beta}\right)\right] \\ & +\epsilon_2(\infty)\frac{(\omega_{l2}^2-\omega_{t2}^2)}{(\omega^2-\omega_{t2}^2)^2}[\sinh(\beta L_z/2)]^{-2} \\ & \times\left[\alpha^2\left(\frac{\sinh(\beta L_z)}{\alpha\beta}+\frac{L_z}{\alpha}\right)+\beta^2\left(\frac{\sinh(\beta L_z)}{\alpha\beta}\right)\right] \\ & +\epsilon_2(\infty)\frac{(\omega_{l2}^2-\omega_{t2}^2)}{(\omega^2-\omega_{t2}^2)^2}\left(\frac{2(\alpha^2+\beta^2)}{\alpha\beta}\right). \end{aligned} \tag{A14}$$

The parameters α and β are defined by the relations

$$\alpha^2 + \beta^2 - q_x^2 = 0$$
$$\alpha L_y = \beta L_z.$$

The SO phonon frequency ω satisfies the dispersion relation

$$\kappa_1(\omega)\tanh(\tfrac{1}{2}\alpha L_y) + \kappa_2(\omega) = 0$$

for symmetric modes and

$$\kappa_1(\omega)\coth(\tfrac{1}{2}\alpha L_y) + \kappa_2(\omega) = 0$$

for antisymmetric modes. Since only two discrete phonon wave numbers q_x can contribute to electron–phonon scattering in 1D systems (electron scattering back and forth in momentum space), the integration of (A8) over q_x can be replaced by a summation over q_x:

$$\lambda^{e/a}(k_x, j, l; j', l') = \frac{e^2}{8\pi^2\epsilon_o\hbar}\left(\frac{m^*}{2}\right)^{1/2} \sum_{q_x = q_+, q_-} \omega(N + \tfrac{1}{2} \pm \tfrac{1}{2})\, I(q_x, L_y, L_z)\frac{1}{\sqrt{E_x'}} \tag{A15}$$

where $E_x' = E_x + E_{jl} - E_{j'l'} \pm \hbar\omega$ is the electron kinetic energy after scattering, and the phonon wavenumbers q_x can take the values

$$q_\pm^{(e)} = k_x \pm \sqrt{2m^* E_x'}/\hbar \tag{A16}$$

$$q_\pm^{(e)} = -k_x \pm \sqrt{2m^* E_x'}/\hbar. \tag{A17}$$

Here, the initial electron wavenumber $k_x > 0$ for definiteness. Then the plus and minus signs in (A16) and (A17) correspond to forward and backward electron scattering, respectively, for absorption, and to backward and forward scattering, respectively, for emission.

References

[1] Krömer H 1958 *Phys. Rev.* **109** 1856
[2] Krömer H 1960 *Prog. Semicond.* **4** 1
[3] Andronov A A, Dodin E P and Krasil'nik Z F 1982 *Sov. Phys.–Semicond.* **16** 133
[4] Starikov E V and Shiktorov P N 1986 *Sov. Phys.–Semicond.* **20** 677
[5] Dousmanis G C 1958 *Phys. Rev. Lett.* **1** 55
[6] Gershenzon E M, Gurvich Yu L and Litvak-Gorskaya L B 1964 *Ukr. Fiz. Zh.* **9** 948
[7] Andronov A A, Belyantsev A M, Gavrilenko V I, Dodin E P, Krasil'nik Z F, Nikonorov V V and Pavlov S A 1984 *JETP Lett.* **40** 989
[8] Elesin V F and Manykin E A 1966 *Sov. Phys.–JETP* **23** 917
[9] Elesin V F and Manykin E A 1966 *JETP Lett.* **3** 15
[10] Stocker H J 1967 *Phys. Rev. Lett.* **18** 1197
[11] Habegger M A and Fan H Y 1964 *Phys. Rev. Lett.* **12** 99
[12] Stocker H J, Stannard C R Jr, Kaplan H and Levinstein H 1964 *Phys. Rev. Lett.* **12** 163
[13] Benoit a la Guillaume C and Cernogora J 1963 *J. Phys. Chem. Solids* **24** 383

[14] Besfamil'naya V A, Kurova I A, Ormont N N and Ostroborodova V V 1965 *Sov. Phys.–JETP* **21** 1065
[15] Kurova I A and Ormont N N 1965 *Sov. Phys.–Solid State* **6** 2970
[16] Nasledov D N, Popov Yu G and Smetannikova Yu S 1965 *Sov. Phys.–Solid State* **6** 2989
[17] Elesin V F 1968 *JETP Lett.* **7** 176
[18] Aleksandrov A S, Bykovskii Yu A, Elesin V F, Protasov E A and Rodionov A G 1970 *JETP Lett.* **12** 41
[19] Reklaitis A 1983 *Phys. Lett.* **99A** 450
[20] Kim K W, Stroscio M A, Bhatt A, Mickevičius R and Mitin V V 1991 *J. Appl. Phys.* **70** 319
Stroscio M A, Iafrate G J, Kim K W, Littlejohn M A, Goronkin H and Maracas G N 1991 *Appl. Phys. Lett.* **59** 1093
[21] Mickevičius R, Mitin V V, Kim K W, Stroscio M A and Iafrate G J 1992 *J. Phys.: Condens. Matter* **4** 1
[22] Sakaki H 1980 *Japan. J. Appl. Phys.* **19** L735
[23] Fasol G and Sakaki H 1992 *2nd Int. Symp. on New Phenomena in Mesoscopic Structures (Maui, HI, 1992)* p 335
[24] Sakaki H, Noda T, Hirakawa K, Tanaka M and Matsusue T 1987 *Appl. Phys. Lett.* **51** 1934
[25] Lugli P, Molinari E and Rucker H 1991 *Superlatt. Microstruct.* **10** 471